RSC Advances

PAPER

View Article Online
View Journal | View Issue

Cite this: RSC Adv., 2015, 5, 46517

Color tuning and energy transfer in Eu^{2+}/Mn^{2+}-doped $Ba_3Y(PO_4)_3$ eulytite-type orthophosphate phosphors†

Ning Guo,*[a] Chengzheng Jia,[a] Jing Li,[a] Yuefeng Zhao,[a] Ruizhuo Ouyang[a] and Wei Lü[b]

Eulytite-type orthophosphate phosphors $Ba_3Y(PO_4)_3$:Eu^{2+}, Mn^{2+} and $Ba_3Ln(PO_4)_3$:Eu^{2+} (Ln = Lu, Y and Gd) were synthesized by high-temperature solid state reactions under reductive atmospheres. Their photoluminescence showed a surprising red-shift in the emission spectrum with the increase in the ionic radius of Ln in the $Ba_3Ln(PO_4)_3$:Eu^{2+} (Ln = Lu, Y and Gd) phosphors system, which arises from the splitting of the 5d energy level. The phase formation, luminescence properties, and energy-transfer mechanism from the Eu^{2+} to the Mn^{2+} ions, and the CIE coordinates in the $Ba_3Y(PO_4)_3$:Eu^{2+}, Mn^{2+} phosphors were investigated. From powder X-ray diffraction (XRD) analysis, the formation of the single-phased $Ba_3Y(PO_4)_3$ in a cubic crystal system with the space group $I\bar{4}3d$ (no. 220) was confirmed. With the doping of Mn^{2+}, the spectral overlap between the emission spectrum of Eu^{2+} and the excitation spectrum of Mn^{2+} allows resonance-type energy transfer to occur from Eu^{2+} to Mn^{2+} with the mechanism carefully studied by luminescence spectra, energy transfer efficiency and decay times. By increasing the Mn^{2+} doping concentration in the $Ba_3Y(PO_4)_3$:Eu^{2+}, Mn^{2+} phosphors, the emission colors can be tuned from yellowish-green through yellow and ultimately to orange. Such color tuning emissions originate from the change in intensity between the 4f–5d transitions of the Eu^{2+} ions and the $^4T_1$–$^6A_1$ transitions of the Mn^{2+} ions through the energy transfer from the Eu^{2+} to the Mn^{2+} ions. In particular, compared with the commercial YAG:Ce phosphor, our developed phosphor contains a larger amount of red-emitting component; thus, it possesses favorable properties for application in warm white LEDs.

Received 9th April 2015
Accepted 8th May 2015

DOI: 10.1039/c5ra06347g

www.rsc.org/advances

1. Introduction

White light-emitting diodes (LEDs) have attracted tremendous attention due to their broad application prospects in full-color flat-panel displays, back-lighting sources for liquid-crystal displays and general solid-state lighting sources.[1–6] Currently, the most common approach to realizing white LEDs is to combine an InGaN-based blue diode with yellow-emitting $Y_3Al_5O_{12}$:Ce^{3+} (YAG:Ce) phosphor. However, white LEDs based on YAG:Ce phosphor exhibit an unsatisfactory high correlated color temperature (T_c > 4500 K) and low color rendering indexes (R_a < 80) for general illumination due to the weak emission in the red spectral region.[7–9] In this regard, it is essential to develop orange-yellow-emitting phosphors, which have more emission saturation in the red than YAG:Ce. Although many attempts have been made to develop orange-yellow-emitting phosphors based on nitride and oxynitride, and despite their superior properties, almost all the nitride- and oxynitride-type phosphors require critical preparation conditions, such as high temperature, high pressure, and carbothermal reactions,[10–12] which limit their application. Therefore, it is important to develop oxide-type orange-yellow-emitting phosphors using comparatively mild synthesis routes for white LEDs.

Recently, eulytite-type orthophosphate compounds with the general composition $M_3Ln(PO_4)_3$ (M = alkaline earth; Ln = trivalent rare earth) have been extensively reported as a suitable phosphor host due to their excellent thermal stability, simple synthesis conditions, and good optical properties when doped with rare-earth activators.[13–15] In the compound $M_3Ln(PO_4)_3$, the Ln^{3+}/M^{2+} pairs of cations are disordered on a single crystallographic site (C_3 point group symmetry), while the oxygen atoms of the phosphate groups are distributed over several partially occupied sites. This type of compound was found to show not only disorder in the cation but also an oxygen sub-lattice disorder.[16–18] Thus, this disordered structure provides a family of sites for the doping ions to occupy. Therefore, it is worth studying new efficient oxide-type orange-yellow-emitting

[a]Department of Chemistry, School of Science, University of Shanghai for Science and Technology, Shanghai 200093, P. R. China. E-mail: guoning@usst.edu.cn; Fax: +86-21-65711344; Tel: +86-21-65711344

[b]State Key Laboratory of Rare Earth Resource Utilization, Changchun Institute of Applied Chemistry, Chinese Academy of Sciences, Changchun 130022, P. R. China

† Electronic supplementary information (ESI) available: The crystal structure of $Ba_3Y(PO_4)_3$ viewed along [100] direction (Fig. S1). The coordination environment of Ba/Y viewed along [111] direction (Fig. S2). The coordination environment of P viewed along [100] direction (Fig. S3). Comparison of the integral area of the four Gaussian components for $Ba_3Ln(PO_4)_3$:Eu^{2+} (Table S1). See DOI: 10.1039/c5ra06347g

luminescent materials with structures derived from eulytite-type compounds. These facts prompted us to study the luminescence properties of $Ba_3Y(PO_4)_3$ activated by Eu^{2+} and Mn^{2+} ions. In addition, to the best of our knowledge, the effect of Eu^{2+}- and Mn^{2+}-doping in the $Ba_3Y(PO_4)_3$ host has not been reported to date.

In this study, a series of orange-yellow-emitting eulytite-type orthophosphate phosphors, $Ba_3Y(PO_4)_3$:Eu^{2+}, Mn^{2+} (BYP:Eu^{2+}, Mn^{2+}), were prepared by a conventional solid-state reaction. The photoluminescence excitation and emission spectra, energy transfer mechanism, and color tuning properties were investigated in detail. In particular, the luminescent properties of the $Ba_3Ln(PO_4)_3$:Eu^{2+} (Ln = Lu, Y and Gd) phosphor system are discussed in terms of crystal field strength and the Eu–O bond.

2. Experimental section

2.1. Materials and synthesis

The powder samples $Ba_{3(1-x-y)}Y(PO_4)_3$:xEu^{2+}, yMn^{2+} (BYP:xEu^{2+}, yMn^{2+}) and $Ba_3Ln(PO_4)_3$:Eu^{2+} (Ln = Lu, Y and Gd) were synthesized by a solid-state reaction method. The reactants $BaCO_3$ (A.R. (Analytical Reagent)), Ln_2O_3 (Ln = Lu, Y and Gd; 99.99%), $NH_4H_2PO_4$ (A.R.), Eu_2O_3 (99.99%) and $MnCO_3$ (A.R.) were weighed according to stoichiometric ratio. After mixing and grinding, the mixtures were heated at 1300 °C for 4 h under a 10% H_2–90% N_2 gas mixture. Finally, the as-synthesized samples were slowly cooled to room temperature.

2.2. Measurements and characterization

The phase purity of the obtained phosphors were carefully checked using powder X-ray diffraction (XRD) analysis (Bruker AXS D8) in the 2θ range from 10° to 80° with graphite monochromatized Cu Kα radiation (λ = 0.15405 nm) operating at 40 kV and 40 mA. A step size of 0.02° (2θ) was used with a scanning speed of 10° min^{-1} in the 2θ range. The photoluminescence emission (PL) and photoluminescence excitation (PLE) spectra of the obtained powders were recorded with a Hitachi F-4500 spectrophotometer equipped with a 150 W xenon lamp as the excitation source. The luminescence decay curve was obtained from a Lecroy Wave Runner 6100 digital oscilloscope (1 GHz) using a tunable laser (pulse width = 4 ns, gate = 50 ns) as the excitation source (Continuum Sunlite OPO). The quantum efficiency (QE) was analyzed with a PL quantum efficiency measurement system (C9920-02, Hamamatsu Photonics, Shizuoka) containing a 150 W xenon lamp. All the measurements mentioned above were performed at room temperature.

3. Results and discussion

3.1. Phase identification

Fig. 1 shows the powder X-ray diffraction (XRD) patterns of the as-synthesized BYP:0.005Eu^{2+}, yMn^{2+} (y = 0–0.10) samples in contrast to the standard card of $Ba_3Y(PO_4)_3$ (JCPDS 44-0318) for comparison. It was found that all the diffraction peaks of the obtained samples can be indexed to the standard card of $Ba_3Y(PO_4)_3$ and no detectable impurity phase appeared. The results indicate that the introduction of the dopants Eu^{2+}/Mn^{2+} did not cause any significant change in the host structure in our experimental doping-content ranges and the doping ions Eu^{2+}/Mn^{2+} completely entered the host lattice. In addition, one can see that the marked diffraction peak at the 2-theta value of 47.5° was right-shifted to a higher angle with an increase in the Mn^{2+} concentration, which can be ascribed to the successful substitution of the larger Ba^{2+} by the smaller Mn^{2+} ions. The unit cell constants a and V of the BYP:0.005Eu^{2+}, yMn^{2+} (y = 0–0.10) samples were calculated by refining the powder XRD data according to the Rietveld method. From Fig. 2, one can see that the unit cell constants a and V for the BYP:0.005Eu^{2+}, yMn^{2+} samples decreases linearly with an increase in Mn^{2+} concentration, which is consistent with the Vegard's law. The XRD analysis and change in the unit cell constants confirm that the dopants Eu^{2+} and Mn^{2+} have been homogeneously incorporated into the BYP host lattice. In consideration of the effective ionic radii of the cations and the electric charge balances, it was predicted that Eu^{2+} and Mn^{2+} prefer to randomly occupy the Ba^{2+} sites in the BYP host structure.

3.2. Photoluminescence properties

Fig. 3a displays the PLE and PL spectra of the BYP:0.005Eu^{2+} phosphor. The PLE spectra showed a broad absorption between 250 and 420 nm, which was assigned to the $4f^7 \rightarrow 4f^65d^1$ transition of the Eu^{2+} ions. The broad excitation band matches well with the UV LED chips for application in white LEDs. Upon excitation at 350 nm, the PL spectrum comprises several broad bands from 400 to 700 nm, which are attributed to the $4f^65d^1 \rightarrow 4f^7$ transition of the Eu^{2+} ions. The shape of the PL spectrum appears to be asymmetric and broad, indicating that the present host lattice has a family of sites for the Eu^{2+} ions to occupy. The crystal structure of $Ba_3Y(PO_4)_3$ and the coordination environment of the Ba/Y and P are depicted in the ESI.† The $Ba_3Y(PO_4)_3$ host contains two possible different orientations of the $[PO_4]$ tetrahedron, corresponding to the two sets of partially occupied oxygen positions. The Ba^{2+}/Y^{3+} pairs of cations are disordered on a single crystallographic site (C_3 point group symmetry), while the oxygen atoms of the phosphate groups are distributed

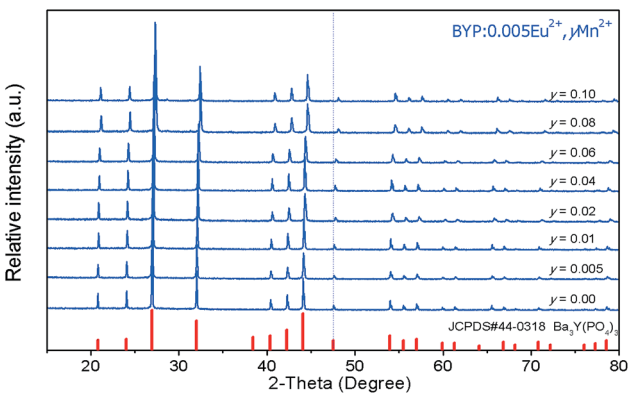

Fig. 1 XRD patterns of the BYP:0.005Eu^{2+}, yMn^{2+} samples. The standard data for $Ba_3Y(PO_4)_3$ (JCPDS card no. 44-0318) is shown as a reference.

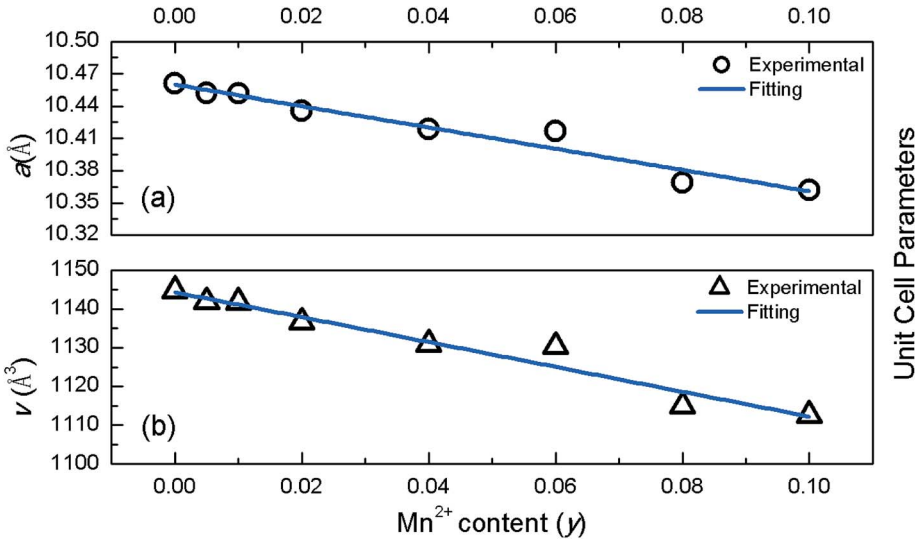

Fig. 2 The relationship between the unit cell constants (*a* and *V*) and Mn^{2+} content (*y*).

over two partially occupied sites. To distinguish the different luminescence sites of the Eu^{2+} ions, the emission curve has been decomposed into four well-separated Gaussian components with peaks at 2.95 eV, 2.40 eV, 2.26 eV, and 2.05 eV (corresponding to 420 nm, 516 nm, 548 nm, and 606 nm, respectively) on an energy scale, as depicted in Fig. 4. These results indicate that there are four luminescence Eu^{2+} centers in the BYP host lattice with different local coordination environments, which is consistent with the fact that the composition of $Ba_3Y(PO_4)_3$ was found to show not only a disorder in the cation but also an oxygen sublattice disorder.[17,18] As shown in Fig. 4, the Eu(B) centered at 2.40 eV (516 nm) may act as the main luminescence center due to its relatively high intensity.

According to the increase in unit cell volume from $Ba_3Lu(PO_4)_3$:Eu^{2+} to $Ba_3Y(PO_4)_3$:Eu^{2+} to $Ba_3Gd(PO_4)_3$:Eu^{2+}, we would expect the crystal field splitting to decrease in the same order, resulting in a blue-shift of the emission wavelength. Instead, as shown in Fig. 5, the $Ba_3Gd(PO_4)_3$:Eu^{2+} compound has the most red-shifted optical properties. The increase in lattice parameters and unit cell volume do not facilitate the prediction of the observed optical properties. Fig. 5 depicts the normalized PL spectra of the $Ba_3Ln(PO_4)_3$:Eu^{2+} (Ln = Lu, Y and Gd) phosphors. The position of the emission peaks is observed to be slightly shifted to a longer wavelength with the successive increase in the radius of the rare-earth metal ions Lu^{3+}, Y^{3+}, and Gd^{3+}. The crystal field strength increases with a decrease in the bond length; the correlation between the crystal field strength and the bond length is $D_q \propto 1/R^5$, where D_q is the crystal field strength and R is the bond length between the central ion and its ligands.[19–21] Accordingly, the increase in the crystal field could lower the 5d excited state energy level and red-shift the emission peaks for the 5d → 4f transition of Eu^{2+}.[22] That is to say, the shorter the Eu–O bond is, the longer the emission wavelength can be observed. As mentioned above, the bond length of Eu–O could be greatly influenced by the surrounding ions due to the disorder of the Eu^{2+}/Ba^{2+}/Ln^{3+} ions at a single C_3 site.[23] In the $Ba_3Ln(PO_4)_3$:Eu^{2+} (Ln = Lu, Y and Gd) phosphor

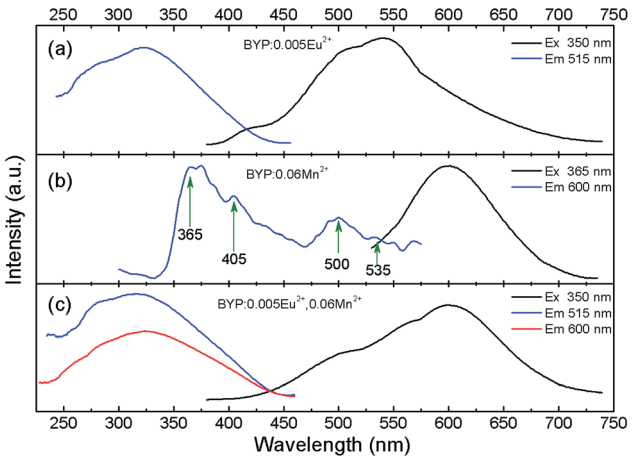

Fig. 3 PLE and PL spectra of (a) the BYP:0.005Eu^{2+} phosphor, (b) the BYP:0.06Mn^{2+} phosphor, and (c) the BYP:0.005Eu^{2+}, 0.06Mn^{2+} phosphor.

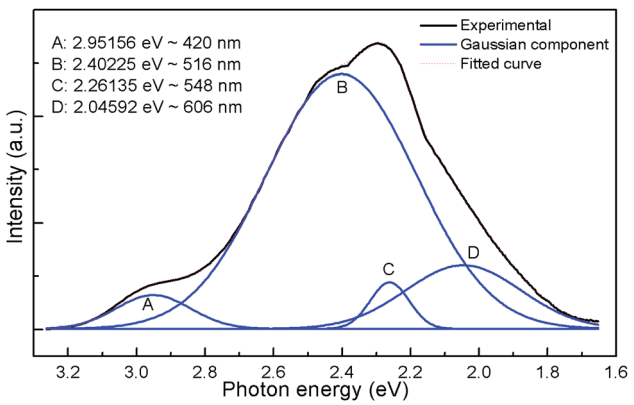

Fig. 4 The emission spectrum of BYP:0.005Eu^{2+} and its corresponding Gaussian components on an energy scale.

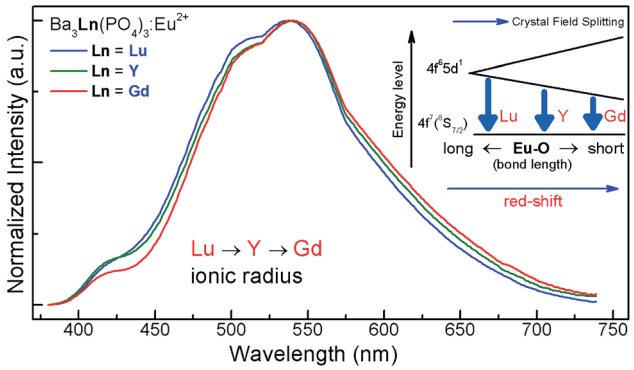

Fig. 5 The normalized PL spectra of the $Ba_3Ln(PO_4)_3:Eu^{2+}$ (Ln = Lu, Y and Gd) phosphors. The inset shows the schematic energy level diagram of Eu^{2+} ions in the $Ba_3Ln(PO_4)_3$ host lattice.

system, the large ionic radii of the Gd^{3+} ions leads to a stressful compression of the neighboring Eu–O bonds when Ln = Gd, while in the $Ba_3Lu(PO_4)_3:Eu^{2+}$ phosphor, some stress is released owing to the smaller ionic radius of Lu^{3+} than that of Gd^{3+}, and thus the bond length of Eu–O becomes longer. This result indicates the highest degree of distortion in $Ba_3Gd(PO_4)_3:Eu^{2+}$, confirming that this compound has the most red-shifted optical properties. The increased degree of distortion causes a larger crystal field splitting. As shown in the inset of Fig. 5, as the ionic radii of Lu, Y and Gd are successively increased, the crystal field splitting becomes larger with a decrease in the Eu–O bond length, leading to a different decrease between the 4f and 5d energy levels of the Eu^{2+} ions. As a result, a red shift of the emission peak is caused with an increase in the ionic radius of Ln in the $Ba_3Ln(PO_4)_3:Eu^{2+}$ (Ln = Lu, Y and Gd) phosphor system. Furthermore, the Eu^{2+} ions that occupy different sites may also contribute to this red shift. Table S1 (See ESI†) displays the integral area of the four Gaussian components (A, B, C, and D) for $Ba_3Ln(PO_4)_3:Eu^{2+}$ (Ln = Lu, Y and Gd) phosphors. One can see that the integral area of the PL spectrum for the A and B sites decrease, while the integral area for the D site increases from Lu to Y and eventually to Gd. The change in the integral area of the four Gaussian components (A, B, C, and D) is consistent with this red shift.

Fig. 3b depicts the PLE and PL spectra of $BYP:0.06Mn^{2+}$. The PLE spectrum shows several distinct peaks centered at 365, 405, 500, and 535 nm, which were assigned to the d–d transition of the Mn^{2+} ion from the ground level $^6A_1(^6S)$ to the $^4T_2(^4D)$, $[^4A_1(^4G)$, $^4E(^4G)]$, $^4T_2(^4G)$, and $^4T_1(^4G)$ excited levels, respectively.[24,25] Upon excitation at 365 nm, the PL spectrum exhibits a broad emission band centered at 600 nm, which can be ascribed to the spin-forbidden d–d transition from $^4T_1(^4G)$ to the ground state $^6A_1(^6S)$ of Mn^{2+} ions. Mn^{2+}-doped phosphors typically exhibit a broad emission band, and the emission wavelength depends strongly on the crystal-field strength of the host lattice. The stronger the crystal field is, the longer emission wavelength is expected to be observed. At the same time, the coordination number also has a great effect on the emission color.[24] Thus, the appearance of the reddish-orange emission band of the Mn^{2+} ions indicates that the Mn^{2+} ions substitute the Ba^{2+} sites. Because the d–d transition in Mn^{2+} centers is at parity and spin-forbidden, its excitation intensity is not sufficiently high in the UV wavelength regions.[25] Therefore, co-dopants such as Eu^{2+} or Ce^{3+} are often added to increase the sensitizing action of the crystal lattice.

To enhance the absorption of the samples in the UV region, the dopant Eu^{2+} is expected to act as a sensitizer to transfer energy to the Mn^{2+} ions. As shown in Fig. 3a and b, by comparing the PL spectrum of the $BYP:0.005Eu^{2+}$ and the PLE spectrum of $BYP:0.06Mn^{2+}$, an apparent spectral overlap can be observed. On the basis of the Dexter's theory,[26] an effective resonance type energy transfer is expected to take place from the Eu^{2+} to the Mn^{2+} ions. This can be further confirmed by the PL and PLE spectra of $BYP:0.005Eu^{2+}$, $0.06Mn^{2+}$, as shown in Fig. 3c. For the Eu^{2+} and Mn^{2+} codoped sample, upon excitation into the PLE band of the Eu^{2+} ions, the PL spectrum consists of a yellowish-green band, assigned to the f–d transitions of the Eu^{2+} ions, and a reddish-orange band, attributed to the $^4T_1$–$^6A_1$ transitions of the Mn^{2+} ions. In addition, one can see that the PLE spectrum monitoring the emission of the Mn^{2+} is similar to that monitoring the emission of the Eu^{2+} ions, demonstrating the existence of energy transfer from the Eu^{2+} to the Mn^{2+} ions.[27,28] Based on the discussion above, it can be concluded that Eu^{2+} ions can be excited by UV irradiation and that they strongly absorb the energy and then transfer the energy to Mn^{2+}. Therefore, the emission from both Eu^{2+} and Mn^{2+} can be observed in a single host.

Fig. 6 depicts the PL spectra of the $BYP:0.005Eu^{2+}$, yMn^{2+} samples with a fixed Eu^{2+} content of 0.005 and a varying Mn^{2+} content y in the range of 0–0.10. Upon excitation at 350 nm, the PL spectra exhibit several broad emission bands, which can be ascribed to the emission of Eu^{2+} and Mn^{2+}. Thus, we can adjust the relative intensity of the emission bands by tuning the amounts of the activator, and a multicolor emission can be obtained in a single host through the principle of energy transfer. From Fig. 6, one can see that the PL intensity for Eu^{2+} decreases monotonically with an increase in the Mn^{2+} doping content. Moreover, the reddish-orange emission of the Mn^{2+} ions increases initially until it reaches a maximum at $y = 0.06$, beyond which it decreases, which is ascribed to the Mn^{2+}–Mn^{2+} internal concentration quenching. The observed variations in the emission intensity of the Eu^{2+} and Mn^{2+} ions strongly indicate the energy transfer from Eu^{2+} to Mn^{2+}. Moreover, as shown in the inset of Fig. 6, one can see that the emission peak of the Mn^{2+} ions shifts toward long-wavelength from 576 to 611 nm with an increase of the Mn^{2+} content y from 0.005 to 0.10, which could be assigned to the change of the crystal field strength. Because the radius of the Mn^{2+} ions is smaller than that of Ba^{2+} ions, the crystal lattice of BYP shrinks after doping Mn^{2+} ions into the BYP host lattice to replace Ba^{2+} ions, as confirmed by the shift of XRD pattern to higher angles, and then the unit cell constants for the $BYP:0.005Eu^{2+}$, yMn^{2+} samples decrease linearly with the increase in Mn^{2+} content (Fig. 1 and 2). This leads to the enhancement of the crystal field strength surrounding the Mn^{2+} ions and further results in a larger crystal field splitting of the Mn^{2+} 3d energy levels, which brings the

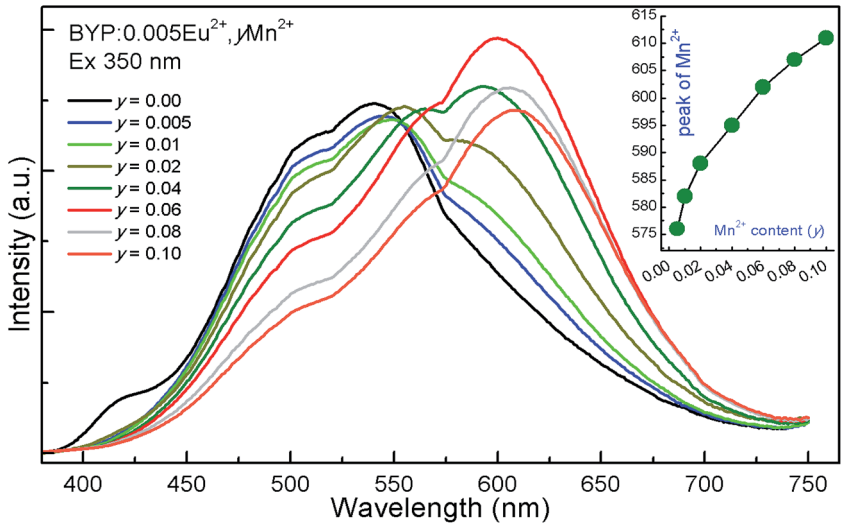

Fig. 6 PL spectra for the BYP:0.005Eu^{2+}, yMn^{2+} phosphors with varying Mn^{2+} doping content (y). The inset shows the dependence of the emission peak of the Mn^{2+} on Mn^{2+} content (y).

lowest 3d state of Mn^{2+} closer to its ground state, and finally gives a red shift to the PL emission peak of the Mn^{2+} ion.[24,25]

To further explore the energy transfer processes and energy transfer efficiency from the Eu^{2+} to the Mn^{2+} ion, the fluorescence decay curves of Eu^{2+} in the BYP:0.005Eu^{2+}, yMn^{2+} samples, monitoring the emission of Eu^{2+} at 516 nm, were measured and investigated, as depicted in Fig. 7. It should be noted that the decay curves in the single Eu^{2+}-doped BYP:0.005Eu^{2+} sample deviate from a single exponential, indicating that there is more than one luminescent Eu^{2+} center in the host lattice, which is also consistent with the crystal structure of the host lattice. From Fig. 7, one can see that all the decay curves of Eu^{2+} in the BYP:0.005Eu^{2+}, yMn^{2+} ($y = 0$–0.10) samples deviate from a single exponential rule, and this deviation is more evident with an increase in the Mn^{2+} doping concentration. Because of the non-exponential decay of Eu^{2+} in all the samples, the average fluorescence lifetime of Eu^{2+} has been defined as follows:[29,30]

$$\tau_{avg} = \int_0^\infty I(t)t\mathrm{d}t \Big/ \int_0^\infty I(t)\mathrm{d}t \quad (1)$$

where $I(t)$ is the fluorescence intensity at time t. Based on eqn (1), the average fluorescence lifetimes of Eu^{2+} were calculated and are depicted on the left axis in Fig. 8. It can be observed that the lifetime of the Eu^{2+} in the BYP:0.005Eu^{2+}, yMn^{2+} ($y = 0$–0.10) samples decrease monotonically with an increase in the Mn^{2+} doping concentration, further confirming the energy transfer from Eu^{2+} to Mn^{2+} in the BYP:0.005Eu^{2+}, yMn^{2+} samples. Assuming that all the excited Mn^{2+} ions decay radioactively, the energy transfer efficiency (η_T) from Eu^{2+} to Mn^{2+} can be obtained according to the data of the average lifetimes by the following equation:[31]

$$\eta_T = 1 - \tau/\tau_0 \quad (2)$$

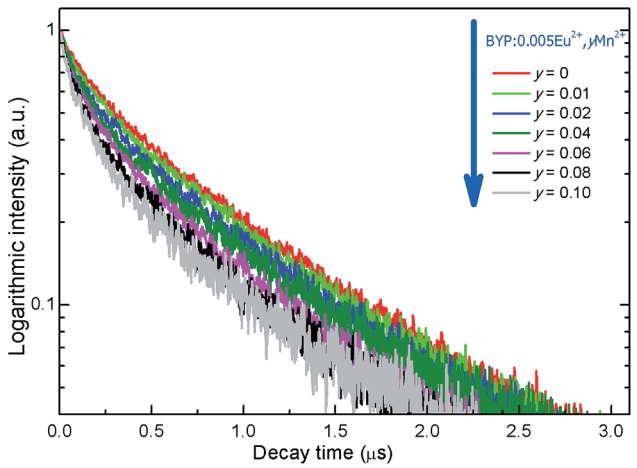

Fig. 7 Photoluminescence decay curves of Eu^{2+} in the BYP:0.005Eu^{2+}, yMn^{2+} phosphors displayed on a logarithmic intensity scale (excited at 355 nm, monitored at 516 nm).

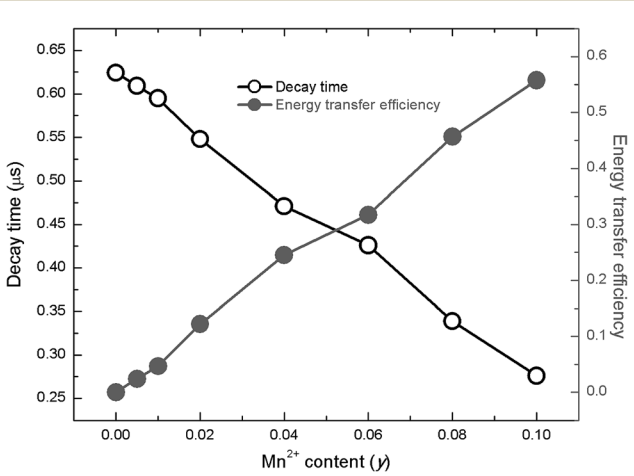

Fig. 8 Dependence of the energy transfer efficiency η_T and the fluorescence lifetime of Eu^{2+} on the Mn^{2+} content (y).

where τ and τ_0 are the decay times of the sensitizer Eu^{2+} in the presence and absence of the activator Mn^{2+}, respectively. Accordingly, the energy transfer efficiencies (η_T) were calculated as a function of the Mn^{2+} content, and are also illustrated in Fig. 8. As shown on the right axis in Fig. 8, one can see that the energy transfer efficiency from Eu^{2+} to Mn^{2+} increases gradually as the content of Mn^{2+} increases from 0 to 0.10. At $y = 0.10$ in the BYP:0.005Eu^{2+}, $y$$Mn^{2+}$ samples, the energy transfer efficiency can reach 55.8%. This suggests that the energy transfer efficiency from Eu^{2+} to Mn^{2+} is partial and depends strongly on the Mn^{2+} doping content. Compared with Ce^{3+}–Tb^{3+} and Ce^{3+}–Mn^{2+} codoped eulytite-type phosphors,[32,33] the energy transfer efficiency from Eu^{2+} to Mn^{2+} in the BYP:0.005Eu^{2+}, $y$$Mn^{2+}$ samples is relatively low. The main reason for this may be attributed to the small spectral overlap between the emission band of Eu^{2+} and the excitation band of Mn^{2+} in the BYP:Eu^{2+}, Mn^{2+} phosphors.

In general, the energy transfer between the Eu^{2+} and Mn^{2+} ions mainly takes place *via* an exchange interaction and electric multipolar interaction. According to the Dexter's energy transfer formula for exchange and multipolar interactions, the following relation can be given:[34–36]

$$\ln(I_0/I) \propto C \quad (3)$$

$$\frac{I_0}{I} \propto C^{n/3} \quad (4)$$

where I and I_0 are the integrated emission intensities of the PL spectrum for the sensitizer Eu^{2+} in the presence and absence of the activator Mn^{2+}, respectively, and C is the sum doping concentration of Eu^{2+} and Mn^{2+}. The linear relationship $\ln(I_0/I) - C$ corresponds to the exchange interaction, and $(I_0/I) - C^{n/3}$ with $n = 6$, 8, and 10 corresponds to the dipole–dipole, dipole–quadrupole, and quadrupole–quadrupole interactions, respectively. The relationships of $\ln(I_0/I) - C$ and $(I_0/I) - C^{n/3}$ are illustrated in Fig. 9. A liner relation is observed when $n = 8$. This clearly indicates that the dominant interaction mechanism for the Eu–Mn energy transfer in the BYP host is based on the dipole–quadrupole interaction, which is similar to that previously investigated and observed for $Sr_3Lu(PO_4)_3$:Eu^{2+}, Mn^{2+},[14] $Sr_3La(PO_4)_3$:Eu^{2+}, Mn^{2+} (ref. 37) and $Ba_3Lu(PO_4)_3$:Eu^{2+}, Mn^{2+}.[38]

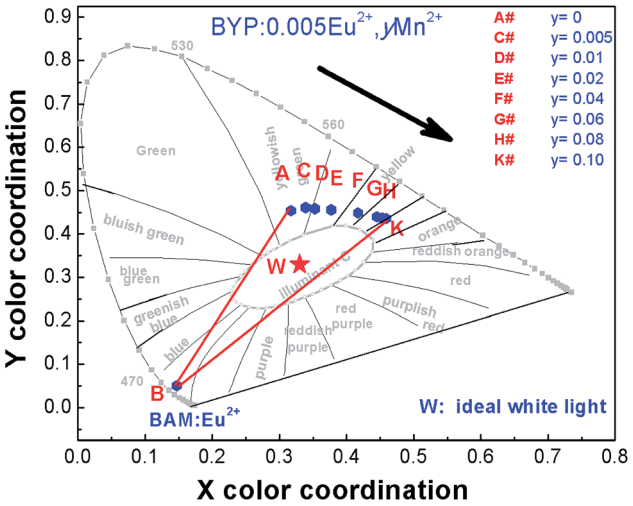

Fig. 10 CIE chromaticity diagram for the BYP:0.005Eu^{2+}, $y$$Mn^{2+}$ phosphors excited at 350 nm.

The Commission Internationale de L'Eclairage (CIE) chromaticity coordinates of the BYP:0.005Eu^{2+}, $y$$Mn^{2+}$ phosphors with varying Mn^{2+} concentration were determined based on their relevant PL spectrum, and are depicted in Fig. 10 and

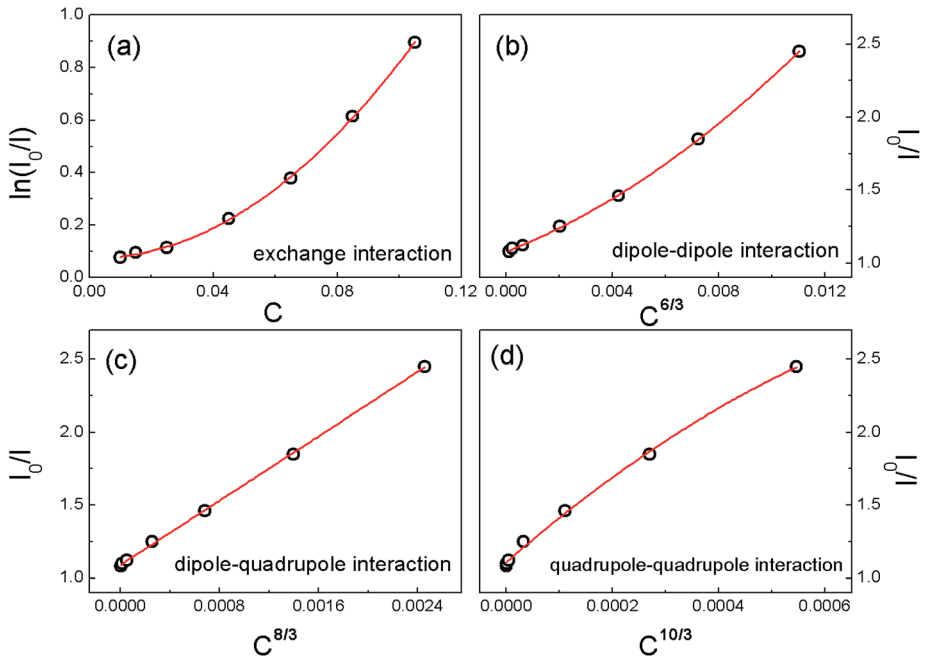

Fig. 9 (a) Dependence of $\ln(I_0/I)$ of Eu^{2+} on C; and I_0/I of Eu^{2+} on (b) $C^{6/3}$, (c) $C^{8/3}$, and (d) $C^{10/3}$.

Table 1 Comparison of the CIE chromaticity coordinates (*x*, *y*), emissive colors, and quantum efficiency (QE) for the BYP:0.005Eu^{2+}, *y*Mn^{2+} phosphors excited at 350 nm

Sample no.	Sample composition (*y*)	CIE coordinates (*x*, *y*)	Emissive colors	Quantum efficiency (QE)
A	0	(0.321, 0.456)	Yellowish-green	17%
C	0.005	(0.342, 0.461)	Yellowish-green	19%
D	0.01	(0.356, 0.459)	Yellow	15%
E	0.02	(0.381, 0.456)	Yellow	20%
F	0.04	(0.413, 0.449)	Yellow	15%
G	0.06	(0.439, 0.441)	Orange	23%
H	0.08	(0.450, 0.437)	Orange	14%
K	0.10	(0.457, 0.436)	Orange	12%

Table 1. The Eu^{2+} doping content was fixed at 0.005 as the concentration of Mn^{2+} was increased from 0 to 0.10; through the energy transfer of $Eu^{2+} \rightarrow Mn^{2+}$, the corresponding color tone of the BYP:0.005Eu^{2+}, *y*Mn^{2+} phosphor shifts from yellowish-green through yellow and ultimately to orange. Accordingly, UV-pumped white LEDs with improved chromaticity quality can be fabricated using a UV-LED chip with our developed BYP:0.005Eu^{2+}, *y*Mn^{2+} phosphor system and the blue-emitting BAM:Eu^{2+} ($BaMgAl_{10}O_{17}$:Eu^{2+}) phosphor. Consequently, it is clear that white LEDs with tunable correlated color temperature (CCT) in the triangle ABK region (Fig. 10) can be produced to meet the needs of different illumination applications by simply varying the Mn^{2+} doping concentration (*y*) in the BYP:0.005Eu^{2+}, *y*Mn^{2+} phosphor system. In particular, compared with the commercial YAG-based white LED system, these UV-pumped white LEDs can produce warm white light with low CCT, which is more suitable for room lighting. This is mainly due to the as-developed phosphor, which contains more red-emitting component than YAG:Ce. In addition, it should be noted that the experimental conditions and reactants composition should be optimized to improve the quantum efficiency.

4. Conclusion

In summary, a series of eulytite-type orthophosphate phosphors $Ba_3Y(PO_4)_3$:Eu^{2+}, Mn^{2+} and $Ba_3Ln(PO_4)_3$:Eu^{2+} (Ln = Lu, Y and Gd) were synthesized *via* a high-temperature solid-state reaction process. In the order of Lu, Y, and Gd for the $Ba_3Ln(PO_4)_3$:Eu^{2+} (Ln = Lu, Y and Gd) phosphor system, a red shift of the emission peak is caused with increases in the ionic radius owing to the increase in the crystal field strength. The energy transfer from the Eu^{2+} to the Mn^{2+} ions in the BYP:Eu^{2+}, Mn^{2+} phosphors was confirmed to occur *via* a dipole–quadrupole mechanism by the Dexter theoretical model. Upon the excitation of UV light, the emissive colors of the obtained phosphors could be tuned from yellowish-green through yellow and ultimately to orange through energy transfer by adjusting the doping content ratio between Eu^{2+} and Mn^{2+}. In particular, an orange emission with CIE coordinates of (0.439, 0.441) and a QE of 23% could be achieved in the BYP:0.005Eu^{2+}, 0.06Mn^{2+} phosphor. A red-shift emission of the Mn^{2+} ions toward long-wavelength from 576 to 611 nm was observed in the BYP:0.005Eu^{2+}, *y*Mn^{2+} phosphor system with the increase of Mn^{2+} content *y* from 0.005 to 0.10, which could be assigned to the change of the crystal field strength. The energy transfer efficiency increases gradually as the content of Mn^{2+} increases; at $y = 0.10$, the energy transfer efficiency can reach 55.8%. This suggests that the energy transfer efficiency from Eu^{2+} to Mn^{2+} is partial and depends strongly on the Mn^{2+} doping content.

Acknowledgements

This work is financially supported by the National Natural Science Foundation of China (Grant no. 21401130), the Opening Research Fund of the State Key Laboratory of Rare Earth Resource Utilization, Changchun Institute of Applied Chemistry, Chinese Academy of Sciences (RERU2014005).

References

1 X. Bai, G. Caputo, Z. D. Hao, V. T. Freitas, J. H. Zhang, R. L. Longo, O. L. Malta, R. A. S. Ferreira and N. Pinna, *Nat. Commun.*, 2014, **5**, 5702.
2 D. Zhang, L. Duan, Y. Zhang, M. Cai, D. Zhang and Y. Qiu, *Light: Sci. Appl.*, 2015, **4**, e232.
3 A. Marchuk and W. Schnick, *Angew. Chem., Int. Ed.*, 2015, **54**, 2383–2387.
4 Y. Sato, H. Kato, M. Kobayashi, T. Masaki, D.-H. Yoon and M. Kakihana, *Angew. Chem., Int. Ed.*, 2014, **53**, 7756–7759.
5 X. Li, J. D. Budai, F. Liu, J. Y. Howe, J. Zhang, X.-J. Wang, Z. Gu, C. Sun, R. S. Meltzer and Z. Pan, *Light: Sci. Appl.*, 2013, **2**, e50.
6 J. H. Oh, S. J. Yang and Y. R. Do, *Light: Sci. Appl.*, 2014, **3**, e141.
7 P. Li, Z. Wang, Q. Guo and Z. Yang, *RSC Adv.*, 2015, **5**, 4448–4453.
8 N. Chouhan, C. C. Lin, S.-F. Hu and R.-S. Liu, *J. Mater. Chem. C*, 2015, **3**, 1473–1479.
9 A. A. Setlur, E. V. Radkov, C. S. Henderson, J. H. Her, A. M. Srivastava, N. Karkada, M. S. Kishore, N. P. Kumar, D. Aesram, A. Deshpande, B. Kolodin, L. S. Grigorov and U. Happek, *Chem. Mater.*, 2010, **22**, 4076–4082.
10 P. Pust, V. Weiler, C. Hecht, A. Tucks, A. S. Wochnik, A. K. Henss, D. Wiechert, C. Scheu, P. J. Schmidt and W. Schnick, *Nat. Mater.*, 2014, **13**, 891–896.

11 C. Hecht, F. Stadler, P. J. Schmidt, J. S. A. der Guenne, V. Baumann and W. Schnick, *Chem. Mater.*, 2009, **21**, 1595–1601.
12 R.-J. Xie and N. Hirosaki, *Sci. Technol. Adv. Mater.*, 2007, **8**, 588–600.
13 P. L. Li, Z. J. Wang, Z. P. Yang and Q. L. Guo, *J. Electrochem. Soc.*, 2012, **159**, H307–H311.
14 N. Guo, Y. Zheng, Y. Jia, H. Qiao and H. You, *J. Phys. Chem. C*, 2012, **116**, 1329–1334.
15 Y. C. Jia, W. Lu, N. Guo, W. Z. Lu, Q. Zhao and H. P. You, *Chem. Commun.*, 2013, **49**, 2664–2666.
16 J. Barbier, J. E. Greedan, T. Asaro and G. J. McCarthy, *Eur. J. Solid State Inorg. Chem.*, 1990, **27**, 855–867.
17 J. Barbier, *J. Solid State Chem.*, 1992, **101**, 249–256.
18 E. Arbib, B. Elouadi, J. P. Chaminade and J. Darriet, *Mater. Res. Bull.*, 2000, **35**, 761–773.
19 P. Dorenbos, *J. Lumin.*, 2003, **104**, 239–260.
20 P. Dorenbos, *J. Alloys Compd.*, 2002, **341**, 156–159.
21 J. S. Kim, P. E. Jeon, J. C. Choi and H. L. Park, *Solid State Commun.*, 2005, **133**, 187–190.
22 Z. Xia, Y. Zhang, M. S. Molokeev, V. V. Atuchin and Y. Luo, *Sci. Rep.*, 2013, **3**, 3310.
23 Z. Wang, Z. Xia, M. S. Molokeev, V. V. Atuchin and Q. Liu, *Dalton Trans.*, 2014, 16800–16804.
24 G. Q. Yao, J. H. Lin, L. Zhang, G. X. Lu, M. L. Gong and M. Z. Su, *J. Mater. Chem.*, 1998, **8**, 585–588.
25 L. A. Shi, Y. L. Huang and H. J. Seo, *J. Phys. Chem. A*, 2010, **114**, 6927–6934.
26 D. L. Dexter, *J. Chem. Phys.*, 1953, **21**, 836–850.
27 Y. Liu, X. Zhang, Z. Hao, X. Wang and J. Zhang, *Chem. Commun.*, 2011, **47**, 10677–10679.
28 D. W. Wen, J. J. Feng, J. H. Li, J. X. Shi, M. M. Wu and Q. Su, *J. Mater. Chem. C*, 2015, **3**, 2107–2114.
29 N. Guo, Y. Huang, H. You, M. Yang, Y. Song, K. Liu and Y. Zheng, *Inorg. Chem.*, 2010, **49**, 10907–10913.
30 N. Guo, H. P. You, C. Z. Jia, R. Z. Ouyang and D. H. Wu, *Dalton Trans.*, 2014, 12373–12379.
31 P. I. Paulose, G. Jose, V. Thomas, N. V. Unnikrishnan and M. K. R. Warrier, *J. Phys. Chem. Solids*, 2003, **64**, 841–846.
32 T. W. Kuo and T. M. Chen, *J. Electrochem. Soc.*, 2010, **157**, J216–J220.
33 Z. Wang, S. Lou and P. Li, *J. Lumin.*, 2014, **156**, 87–90.
34 D. L. Dexter and J. H. Schulman, *J. Chem. Phys.*, 1954, **22**, 1063–1070.
35 G. Blasse, *Philips Res. Rep.*, 1969, **24**, 131–144.
36 R. Reisfeld and N. Lieblich-Soffer, *J. Solid State Chem.*, 1979, **28**, 391–395.
37 X. G. Zhang, P. He, L. Y. Zhou, Q. Pang, J. X. Shi and M. L. Gong, *J. Lumin.*, 2015, **157**, 352–356.
38 N. Guo, Y. J. Huang, Y. C. Jia, W. Z. Lv, Q. Zhao, W. Lu, Z. G. Xia and H. P. You, *Dalton Trans.*, 2013, 941–947.